Mechanics of Materials 43 (2011) 556–566

Contents lists available at ScienceDirect

Mechanics of Materials

journal homepage: www.elsevier.com/locate/mechmat

Coupling effect of primary voids and secondary voids on the ductile fracture of heat-treatable aluminum alloys

G. Liu [a,b,*], S. Scudino [a], R. Li [a], U. Kühn [a], J. Sun [b], J. Eckert [a,c]

[a] IFW Dresden, Institute for Complex Materials, P.O. Box 270116, D-01171 Dresden, Germany
[b] State Key Laboratory for Mechanical Behavior of Materials, School of Material Science & Engineering, Xi'an Jiaotong University, Xi'an 710049, China
[c] Dresden University of Technology, Institute of Materials Science, D-01062 Dresden, Germany

ARTICLE INFO

Article history:
Received 1 February 2010
Received in revised form 8 May 2011
Available online 3 July 2011

Keywords:
Aluminum alloys
Toughness
Ductility
Voids
Modeling

ABSTRACT

Ductile fracture of commercial aluminum alloys is controlled not only by the primary voids but also by the secondary voids, which are respectively nucleated at cracked constituents and at decohered dispersoid. In this paper, experiment and modeling were carried out to study the combined effect of the two populations of voids on the ductile fracture in two kinds of heat-treatable aluminum alloys, i.e., Al–Cu–Mg alloys and Al–Mg–Si alloys. Different heat treatments were applied to the alloys to achieve various combinations of the two voids, which were subsequently related to the mechanical properties. A multiscale fracture model was proposed to describe quantitatively the relationships between parameters of the two voids and the ductility and fracture toughness of heat-treatable aluminum alloys. It is revealed experimentally and theoretically that the presence of secondary voids will reduce the ductile properties especially when the intervoid spacing is less than about 0.5 μm. All calculations are in good agreement with experimental results.

1. Introduction

Commercial heat-treatable aluminum alloys usually contain multiscale second phase particles (Hahn and Rosenfield, 1975; Staley, 1979; Garrett and Knott, 1978; Thompson, 1975), *i.e.*, coarse constituents with size of 1–10 μm in diameter, intermediate dispersoids of 0.05–0.5 μm in diameter, and fine strengthening precipitates of several tens nanometers in size. Ductile fracture of the aluminum alloys is controlled by these particles. The brittle constituents are ready to crack at lower strain and become large primary voids. Under further deformation, the primary voids grow up to coalescence where the fracture is triggered. The coalescence of primary voids is often rate-limited by the rupture of the intermediate ligament, where the secondary voids caused by dispersoid decohesion play a significant role (Broek, 1973; Van Stone and Psioda, 1975; Haynes and Gangloff, 1998). The secondary voids in aluminum alloys have the size of dispersoids and are one order of magnitude smaller than the primary voids (constituents), agreeing well with the typical definition of secondary voids in ductile metals (see, e.g., Fabregue and Pardoen, 2008). Fig. 1 shows an example of the fracture surface of an Al–Cu–Mg alloy with large primary dimples (primary voids) surrounded by much smaller secondary dimples (secondary voids) nucleated on dispersoids.

The influence of two populations of voids on the elastoplastic deformation of solids has been an attractive topic for many years. Some investigations (Fabregue and Pardoen, 2008; Bandstra and Koss, 2001; Brocks et al., 1995; Faleskog and Shih, 1997; Tvergaard, 1998) have been performed mainly using finite element (FE) based calculations. From these calculations, it was generally revealed that the nucleation and growth of the second population of voids accelerate the damage process and lead to a reduction of ductility. The results can be used to further understand the ductile fracture of elastoplastic solids containing pri-

* Corresponding author at: State Key Laboratory for Mechanical Behavior of Materials, School of Material Science & Engineering, Xi'an Jiaotong University, Xi'an 710049, China.
E-mail address: lgsammer@mail.xjtu.edu.cn (G. Liu).

0167-6636/$ - see front matter © 2011 Elsevier Ltd. All rights reserved.
doi:10.1016/j.mechmat.2011.06.014

Nomenclature

b Burgers vector of aluminum
E, G elastic modulus and shear modulus of aluminum
f_i ($i = c, d, p$) volume fraction of the second phase particles (c: constituent; d: dispersoid; p: precipitate)
J J-integral
L_i($i = c, d, p$) interparticle spacing of the second phase particles (c: constituent; d: dispersoid; p: precipitate); intervoid spacing of primary voids (L_c) and secondary voids (L_d)
n strain hardening exponent
r distance ahead of primary void
r_i ($i = c, d, p$) radius of the second phase particles (c: constituent; d: dispersoid; p: precipitate)
σ_y yield strength
ε^i ($i = d, p$) local strains exerted on adjacent matrix bonded with dispersoids (ε^d) and precipitates (ε^p) during the deformation
ε_y yield strain
ε_{ij} strain tensor
ε_f strain to fracture
ε_p plastic strain
v Poisson's ratio
ρ_i ($i = d, p$) density of geometrically-necessary dislocations due for dispersoids (ρ_d) and precipitates (ρ_p)
ρ_j ($j = t, g, s$) density of total dislocations (ρ_t), of geometrically-necessary dislocations (ρ_g), and of statistically-stored dislocations (ρ_s)
ρ_j^c ($j = t, g$) critical value of ρ_t or ρ_g

mary and secondary voids. However, the FE-based calculation methods are not enough to describe the elastoplastic deformation of aluminum alloys. Firstly, the FE-based methods do not take the dislocation plasticity into account. While in the deformation of aluminum alloys, geometrically necessary dislocations (GNDs) will be progressively induced mainly to accommodate the plastic strain mismatch between precipitates (dispersoids) and surrounding matrix (Ashby, 1970; Russell and Ashby, 1970; Brown and Stobbs, 1976). The significant strengthening contribution from GNDs should not be neglected when calculating the elastoplastic deformation of aged aluminum alloys. Secondly, all the FE-based calculations assumed the pre-existence of the two populations of voids and focused mainly on the coalescence process. While in the practical aluminum alloys, the constituent cracking and dispersoid decohesion are dependent on the matrix strength or the matrix deformation capability. Especially, the nucleation of the secondary voids (or the dispersoid decohesion) is strongly affected by the GNDs that are induced by the deformation incompatibility between dispersoids and plastic matrix (Goods and Brown, 1979). Extensive works (Hahn and Rosenfield, 1975; Staley, 1979; Garrett and Knott, 1978; Thompson, 1975; Hornbogen and Starke, 1993; Walsh et al., 1989; Chen and Knott, 1981) have been carried out to study the separate influence of constituent cracking or dispersoid decohesion on the fracture toughness of aluminum alloys. But few attempts have been made on the coupling effect of the two populations of voids on the ductility and fracture toughness.

In this paper, we attempt to address this deficiency by performing both modeling and experiments. Different combinations of the two voids in Al–Cu–Mg alloys and Al–Mg–Si alloys, were experimentally achieved by elaborately controlling the heat treatments. Different solution + quench treatments (Liu et al., 2005, 2007) were employed to vary content of the constituents and dispersoids in the two alloys, respectively. A serious of aging treatments was subsequently performed to change the alloy strength and deformation capability. The nucleation of both the two voids is strongly dependent on the deformation behavior of the precipitate-containing matrix, besides on the content of constituents and dispersoids. The various combinations of the two voids were quantitatively related to the ductility and fracture toughness of the two alloys. A multiscale fracture model (Liu et al., 2003a, 2004) was pro-

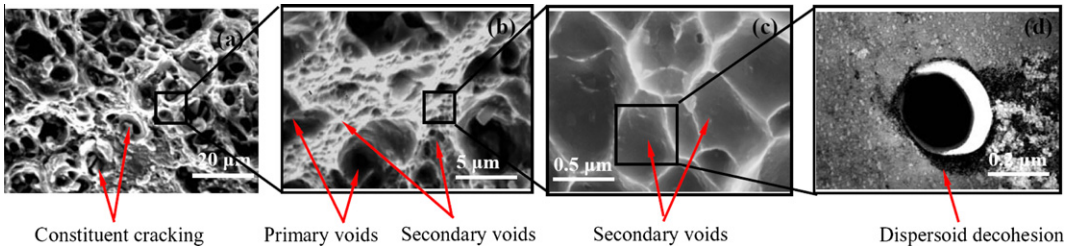

Fig. 1. Typical SEM and TEM images illustrating the dependence of ductile fracture of Al–Cu–Mg alloy on both the primary voids (caused by constituent cracking) and the secondary voids (caused by dispersoid decohesion) in a multi-length manner. (a) Low magnification SEM image on the fracture surface showing the primary voids nucleated on the cracked constituents; (b) large magnification SEM image showing the primary surrounding by small secondary voids; (c) SEM image showing the secondary voids that nucleate on the decohered dispersoids (d) (TEM image). In (c), beam is normal to the local surface using a high angle of tilt.

posed by incorporating the parameters of both primary and secondary voids to calculate the quantitative relationships between the two voids and the ductility and fracture toughness. Calculations were found to fit well with the experimental results and it was revealed experimentally and theoretically that the presence of secondary voids will reduce the ductile properties especially when the intervoid spacing is less than about 0.5 μm. Contours of ductility and fracture toughness in variants of the two voids were developed that can be used to aid the artificial controlling of heat treatments to tailor the combination of the two voids, in order to achieve superior ductile properties for aluminum alloys.

2. Experimental procedure

The aluminum alloys used in present investigation are hot-rolled Al–Cu–Mg plate of 16 mm in thickness and extruded Al–Cu–Mg and Al–Mg–Si rods of both 18 mm in diameter, supplied by the research laboratory of Xi'an air craft industry LTD. The Al–Cu–Mg plate and the Al–Cu–Mg rod are from a same ingot. The composition in weight percentage is 4.62%Cu, 0.65%Mg, 0.22%Mn, 0.08%Si, 0.1%Fe, 0.1%Zn, and balance Al for Al–Cu–Mg alloy and 1.12%Mg, 0.57%Si, 0.25%Cu, and balance Al for Al–Mg–Si alloy, respectively. Both the two alloys contain three types of second phase particles and both fracture surfaces show two populations of voids.

Two experimental approaches are possible to achieve different combinations of two populations of voids and investigate their influence on mechanical properties. One is to change the initial volume fractions of the constituents and/or dispersoids, and the other is to vary the strength as well as the deformation behavior of the matrix. Both can be realized by performing appropriate heat treatments. Based on our previous experimental results (Liu et al., 2005), three types of solution + quench treatments, *i.e.*, enhanced solution + fast quench treatment (abbreviated as EF), traditional solution + fast quench treatment (TF), and traditional solution + slow quenching treatment (TS), were applied on the two aluminum alloys, respectively, to vary the volume fraction of constituents and dispersoids. The enhanced solution or stepped solution was employed to dissolve more soluble constituents and dispersoids as possible while the application of slow quench would cause more constituents and dispersoids. A series of aging treatments were subsequently applied to vary the matrix strength. The detailed heat treatments are as follows. The traditional solution treatments of present Al–Cu–Mg and Al–Mg–Si alloys were held at 766 K for 2 h and at 703 K for half hour, respectively. The fast quenching treatment referred to quench into cold water while the slow quenching treatment means cooling with a controlled rate of 5 K/s. The enhanced solution treatment for Al–Cu–Mg alloy was firstly held at 766 K for 2 h and followed by held at an increasing treatment temperature up to 776 K with a rate of 4 K/h, and for Al–Mg–Si alloy was firstly held at 703 K for half hour and followed by held at an increasing treatment temperature up to 708 K with a rate of 7 K/h. The Al–Cu–Mg alloy and Al–Mg–Si alloy were artificially aged at 483 K, 513 K, 543 K, and at 433 K, 463 K, 493 K, respectively, for various times from 0.25 h to 10 days to get different aging conditions. The maximum error of all the temperature measurements in present experiments was ±1 K. After the heat treatments, the parameters (volume fracture, size, and interparticle spacing) of the three kinds of second phase particles were experimentally determined by using the scanning electron microscope (SEM) and transmission electron microscope (TEM), respectively (Liu et al., 2003a, 2003b).

The stress–strain curves of the samples were recorded and the yield strength (σ_y), tensile strength (σ_s), strain at mechanical instability (ε_s), strain to fracture (ε_f), and strain hardening exponent (n) were determined by using the smooth dog-bone-shaped tensile specimen that has a gauge size of 6 mm in diameter and 40 mm in length. All the specimens had an axis along the longitudinal direction. The tensile test was performed at a constant strain rate of $5 \times 10^{-4}\ s^{-1}$ with the load direction parallel to the specimen axis. The yield stress was determined as the 0.2% offset and the strain to fracture was determined as $\varepsilon_f = \ln(A_o/A_f)$, where A_o is the initial area and A_f is the area at fracture of the specimens. After sample fracture, the fracture surface of the samples was analyzed by using SEM to measure the neatest neighbor spacing of both primary voids and secondary voids, L_c^{exp} and L_d^{exp}, respectively. Using a high angle of tilt, the beam was aligned normal to the local surface for measuring. Different local surfaces have been measured to compile statistic on L_c^{exp} and L_d^{exp}. A magnified local surface for measuring L_d^{exp} is typically shown in Fig. 1(c).

The fracture toughness (K_{IC}) of the Al–Cu–Mg plate samples was characterized with compact tension specimens and the R curve method. Only the L–T oriented specimens, that have a fracture plane whose normal is in the longitudinal direction of the plate and an expected direction of crack propagation coincident with the width direction of the plate, have been measured with applied loading along with the longitudinal direction. All the specimens had a same size of 62.5 mm in width and 6.25 mm in thickness. Prior to the fracture toughness experiment, the specimens were fatigue cracked at a constant stress ratio ($R = K_{min}/K_{max}$) of 0.1 and under decreasing stress intensity condition. Strictly conforming to ASTM E561, the R-curve characterization of fracture toughness was performed on a servohydraulic Instron-type testing machine by using potential-drop method to measure crack length. The crack growth resistance curve was recorded and the plane strain fracture toughness was determined at fracture initiation. All the geometry requirements for plane-strain constraint were met and the obtained plane strain fracture toughness from R-curve has been experimentally found to approximately equal to that determined according to ASTM E399.

3. Experimental results

3.1. Three kinds of second phase particles

Fig. 2(a) and (b) shows the experimental measurements on the volume fracture and size of constituents and

dispersoids in Al–Cu–Mg and Al–Mg–Si alloys, respectively, after different solution + quench treatments. One can see that, comparing with the TF-treated alloys, the EF-treated alloys have reduced volume fraction in both the constituents and the dispersoids, while the TS-treated alloys contain more constituents and dispersoids. This indicates that different initial constituents and dispersoids have been experimentally achieved, which can result in different nucleations of the primary and secondary voids in subsequent testing of the sample.

The precipitate strengthening relies on the volume fraction and size of precipitates that are controlled by the artificial aging treatment. Fig. 3(a) and (b) shows the parameters of precipitates and resultant yield strength in Al–Cu–Mg and Al–Mg–Si alloys, respectively, after peak-aged at different aging temperatures. Dots are experimental measurements and lines are calculations by using strengthening model (Liu et al., 2003b). EF-treated alloys are found to have the highest yield strength because more solute atoms have been dissolved into the matrix after the enhanced solution treatment and more strengthening particles were subsequently precipitated. At the same solution + quench treatments, the alloys aged at low temperature are found to have higher yield strength. This is because the alloys peak-aged at low temperature have finer precipitates than peak-aged at high temperature, which can be also revealed from Fig. 3. The variation in matrix yield strength, which was achieved by performing aging treatment, will cause various combinations of primary and secondary voids even with the same initial constituents and dispersoids.

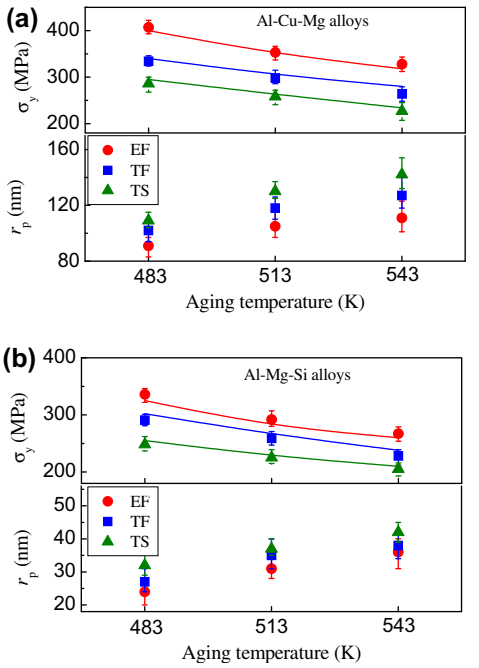

Fig. 3. Dependence of precipitates size (r_p) and yield strength (σ_y) on solution + quench treatments in (a) Al–Cu–Mg alloys and (b) Al–Mg–Si alloys peak-aged at different temperatures. Dots are experimental results and lines on yield strength are calculations from strengthening model [20,21,24].

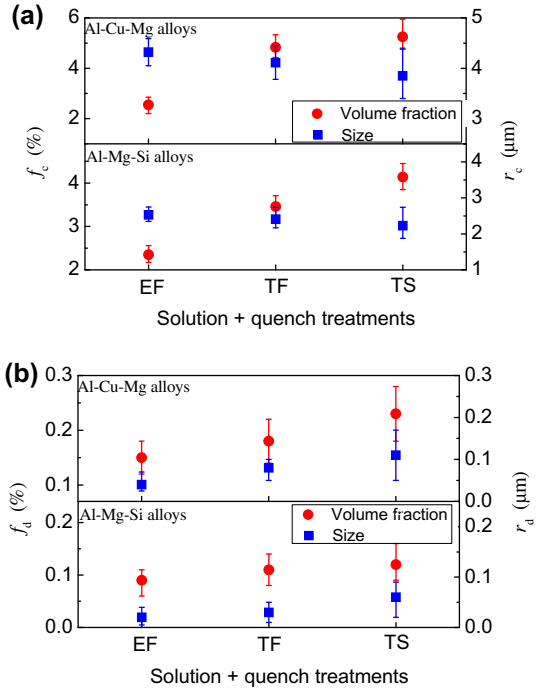

Fig. 2. Evolution of volume fraction (f_i ($i = c, d$)) and particle size (r_i ($i = c, d$)) of constituents (a) and dispersoids (b) with different solution + quench treatments for Al–Cu–Mg alloys and Al–Mg–Si alloys, respectively. EF is enhanced solution + fast quench treatment, TF is traditional solution + fast quench treatment, and TS is traditional solution + slow quench treatment.

3.2. Two populations of voids

Some L_c^{exp} distributions in Al–Cu–Mg alloys are typically shown in Fig. 4 to compare the distribution of primary voids formed under different initial constituents and different matrix strength. Fig. 4(a) shows the comparison among various matrix strengths in EF-treated Al–Cu–Mg alloys, from which it is revealed that the L_c^{exp} distribution in alloys peak-aged at 543 K shifts to the highest average value and that in the alloys peak-aged at 483 K to the lowest one. This indicates that more constituents will crack to form primary voids with increasing the matrix strength. However, when the initial constituents are also changed, the combination effect of initial constituents and matrix strength on the primary voids is much complicated. See the comparison among EF-, TF-, and TS-treated alloys that all peak-aged at 483 K, as shown in Fig. 4(b). Although the TS-treated alloys have lower yield strength than that of the TF-treated ones, the average L_c^{exp} in the two alloys is close. This is because the former alloys have somewhat more initial constituents, which causes the cracked constituents close to those in the latter alloys even under different matrix strength. The EF-treated alloys, however, have the lowest value in L_c^{exp}, due to the much less constituents. Similar results were observed in the Al–Mg–Si alloys, referring to the experimental data summarized in Table 1.

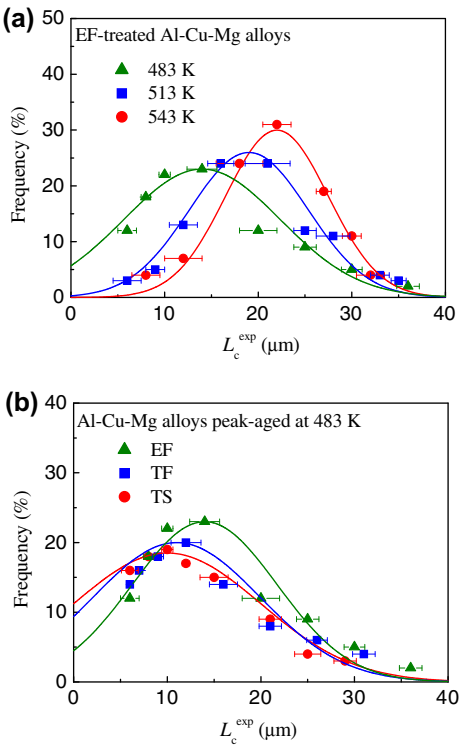

Fig. 4. Nearest neighbor spacing distribution of primary voids (L_c^{exp}) in (a) EF-treated Al–Cu–Mg alloys peak-aged at different temperature and (b) 483 K peak-aged Al–Cu–Mg alloys with different solution + quench treatments. Dots are experimental results and fitting curves are also presented.

As to the secondary voids, some L_d^{exp} distributions in Al–Cu–Mg alloys and Al–Mg–Si alloys are illustratively presented in Fig. 5(a) and (b), respectively. Because there is no significant change in content of dispersoids among the various solution + quench treatments, the secondary voids investigated here are mainly dependent on the matrix strength. Fig. 5 shows that the stronger is the matrix, the more is the dispersoid decohesion and the smaller is L_d^{exp}, which is common to the two kinds of alloys.

3.3. Ductility and fracture toughness

Ductility and fracture toughness of the alloys with different heat treatments are summarized in Table 1. Although it is generally believed that the fracture properties are most sensitive to the coarse second phase particles, the ductility in present experiments is not monotonically changed with L_c^{exp}, see Fig. 6(a) where the TS-treated Al–Cu–Mg alloys have ductility higher than the TF-treated ones when peak-aged at a same temperature. The unusual results are related to the influence of secondary voids. If there is no much difference in L_c^{exp} between two alloys, the alloy having larger L_d^{exp} should has a higher ductility. In such case, the ductility of the alloys will be controlled by L_d^{exp}. This can be used to reasonably explain why the TS-treated alloys have higher ductility than the TF-treated counterparts. On the other hand, the fracture toughness is found to almost increase monotonically with L_c^{exp} in present experiments (Fig. 6(b)). This, however, do not mean that the fracture toughness is predominantly dependent on the primary voids. Actually, the fracture toughness is affected by both primary and secondary voids, which will be discussed later. From Table 1, it is further revealed that the fracture toughness generally increases with reducing the constituents and/or with decreasing the aging temperature (at the same constituents), in agreement with previous observations (Staley, 1979).

4. Discussion

Most recently, a multiscale model (Liu et al., 2003a, 2004, 2005, 2007; Yuan et al., 2007) has been proposed to describe both the separate and coupling effects of the three classes of second phase particles on the ductile fracture of aged aluminum alloys by using a unified expression, where the parameters (e.g., volume fraction, size, and aspect ratio) of all the particles were taken into account (Fig. 7(a)). In this model, the strain to fracture of samples was firstly related to the micro-scaled cracked constituents on basis of the fracture mechanics. Subsequently the critical local strain for rupture of ligament between two neighboring cracked constituents was expressed as a function of the parameters of both submicro-scaled dispersoids and nano-scaled precipitates within the dislocation plasticity description. This makes the multiscale fracture model cover from micrometer scale to nanometer scale and yield a unified expression that is a nonlinear function of the parameters of all the three classes of second phase particles. This multiscale fracture model, however, did not account for the influence of dispersoid decohesion. These will be improved in present model by incorporating the two populations of voids that are dependent not only on the intrinsic characteristics of the particles but also on the deformation behaviors of the matrix.

Referring to Fig. 7(b), the cracked constituents or the primary voids are assumed to arrange in a cubic array, with intervoid spacing of L_c. In the ligament between the neighboring primary voids, dispersoids and precipitates are distributed homogenously. When a percentage P_f^d of the dispersoids are debonded to form secondary voids, the secondary voids have the volume fraction of $f_d P_f^d$ and the intervoid spacing L_d is equal to $r_d\sqrt{4\pi/3f_d P_f^d}$. The number ($N$) of secondary voids distributed between two neighboring primary voids is about $\|L_c/L_d\| + 1$, where the symbol $\|\ \|$ means floor function. The concentration of plastic strain in the matrix ligament located between two neighboring primary voids is induced not only by the strain tensors ahead of the two primary voids but also by the strain tensors ahead of the N secondary voids within the ligament (Fig. 7(c)). The previous multiscale model (Liu et al., 2003a, 2004, 2005; Yuan et al., 2007) is then modified by adding the strain tensors ahead of the secondary voids. When only one secondary void (SV-1 in Fig. 7(c)) is existed between the two neighboring primary voids (PV-1 and PV-2), the strain tensor caused by PV-1, PV-2, and SV-1 at a distance r ahead of PV-1 is respectively given by (Hutchinson, 1968; Rice and Rosengren, 1968)

Table 1
Measurements on the mechanical properties and fracture surface analyses.

Alloys/treatments	L_c^{exp} (μm)	L_d^{exp} (μm)	σ_y (MPa)	φ	ε_s	ε_f	K_{IC} (MPa m$^{1/2}$)	n
Al–Cu–Mg								
543 K								
EF	22.32(4.43)	0.76(0.16)	328(10)	0.30(0.02)	0.17(0.02)	0.36(0.02)	33.26(3.42)	0.12
TF	16.48(3.12)	1.04(0.21)	264(19)	0.25(0.02)	0.13(0.01)	0.29(0.03)	26.78(5.35)	0.14
TS	14.77(3.45)	1.32(0.22)	227(9)	0.28(0.02)	0.11(0.02)	0.33(0.03)	25.06(4.44)	0.15
513 K								
EF	20.15(2.74)	0.63 (0.12)	353(22)	0.25(0.02)	0.13(0.02)	0.29(0.02)	28.43(5.75)	0.11
TF	13.32(1.98)	0.93(0.18)	298(11)	0.21(0.03)	0.10(0.02)	0.24(0.03)	22.68(3.14)	0.12
TS	12.53(3.62)	1.15 (0.24)	258(13)	0.22(0.02)	0.08(0.01)	0.25(0.03)	19.91(4.82)	0.14
483 K								
EF	16.26(3.85)	0.51 (0.08)	407(13)	0.18(0.03)	0.11(0.01)	0.20(0.04)	21.60(6.22)	0.09
TF	12.08(4.02)	0.75(0.17)	334(11)	0.16(0.04)	0.07(0.02)	0.18(0.04)	19.53(4.56)	0.10
TS	10.44(5.75)	0.89 (0.15)	286(10)	0.17(0.02)	0.05(0.01)	0.19(0.03)	17.71(5.32)	0.11
Al–Mg–Si								
493 K								
EF	19.57(2.73)	0.66(0.09)	267(7)	0.33(0.02)	0.20(0.02)	0.40(0.02)	–	0.15
TF	16.25(2.12)	0.97(0.08)	228(9)	0.28(0.02)	0.15(0.03)	0.33(0.03)	–	0.18
TS	15.65(1.45)	1.24(0.06)	205(6)	0.29(0.03)	0.13(0.03)	0.34(0.04)	–	0.19
463 K								
EF	17.25(3.86)	0.54 (0.10)	292(10)	0.29(0.02)	0.16(0.03)	0.34(0.03)	–	0.13
TF	13.37(2.22)	0.88(0.11)	259(7)	0.24(0.03)	0.12(0.01)	0.28(0.03)	–	0.16
TS	12.21(1.57)	1.07(0.08)	225(4)	0.25(0.04)	0.10(0.01)	0.29(0.05)	–	0.18
433 K								
EF	14.68(2.54)	0.42(0.06)	336(5)	0.23(0.03)	0.12(0.02)	0.26(0.04)	–	0.11
TF	11.34(1.99)	0.59(0.11)	291(9)	0.20(0.01)	0.10(0.02)	0.22(0.02)	–	0.14
TS	10.22(1.57)	0.78(0.08)	248(6)	0.21(0.03)	0.07(0.01)	0.23(0.04)	–	0.15

+ – The values in parentheses are standard deviations.

$$\varepsilon_{ij}^{\text{PV-1}} = \alpha\varepsilon_y\left[\frac{J_{\text{PV}}}{\alpha\varepsilon_y\sigma_y I_n r}\right]^{\frac{1}{n+1}}\tilde{\varepsilon}_{ij}(\theta), \tag{1-1}$$

$$\varepsilon_{ij}^{\text{PV-2}} = \alpha\varepsilon_y\left[\frac{J_{\text{PV}}}{\alpha\varepsilon_y\sigma_y I_n (L_c - 2r_c - r)}\right]^{\frac{1}{n+1}}\tilde{\varepsilon}_{ij}(\theta), \tag{1-2}$$

$$\varepsilon_{ij}^{\text{SV-1}} = \alpha\varepsilon_y\left[\frac{J_{\text{SV}}}{\alpha\varepsilon_y\sigma_y I_n (\frac{1}{2}L_c - r_c - r_d - r)}\right]^{\frac{1}{n+1}}\tilde{\varepsilon}_{ij}(\theta), \tag{1-3}$$

where J is the J-integral, ε_y is the yield strain, σ_y is the yield stress, n is the strain hardening exponent, α is the material constant, I_n and $\tilde{\varepsilon}_{ij}(\theta)$ are normalized parameters in the HRR-field (Hutchinson, 1968; Rice and Rosengren, 1968), L_c and r_c are the intervoid (interparticle) spacing and radius of the primary voids (constituent particles), respectively, and r_d is the radius of the secondary voids (dispersoid particles). The J-integral can be separated into two parts, i.e., elastic (J_e) and plastic (J_p) ones. For ductile aluminum alloys, J_e is much smaller than J_p and can be ignored. The J-integral is given by

$$J^{\text{PV}} \approx J_p^{\text{PV}} = \frac{0.405\pi h\sigma_y r_c(\varepsilon_p)^{1+n}}{(\alpha\varepsilon_y)^n}, \tag{2-1}$$

$$J^{\text{SV}} \approx J_p^{\text{SV}} = \frac{0.405\pi h\sigma_y r_d(\varepsilon_p)^{1+n}}{(\alpha\varepsilon_y)^n}. \tag{2-2}$$

Eq. (1) is thus rewritten as

$$\varepsilon_{ij}^{\text{PV-1}} = \Lambda\left(\frac{r_c}{r}\right)^{\frac{1}{1+n}}\varepsilon_p, \tag{3-1}$$

$$\varepsilon_{ij}^{\text{PV-2}} = \Lambda\left(\frac{r_c}{L_c - 2r_c - r}\right)^{\frac{1}{1+n}}\varepsilon_p, \tag{3-2}$$

$$\varepsilon_{ij}^{\text{SV-1}} = \Lambda\left(\frac{r_d}{\frac{1}{2}L_c - r_c - r_d - r}\right)^{\frac{1}{1+n}}\varepsilon_p, \tag{3-3}$$

where $\Lambda = \alpha\varepsilon_y\left[\frac{0.405\pi h}{\alpha\varepsilon_y I_n}\right]^{\frac{1}{1+n}}\tilde{\varepsilon}_{ij}(\theta)$. Adding Eqs. (3-1)–(3-3) and rearranging the new equation leads to

$$\varepsilon_p = \frac{\tilde{\varepsilon}_{ij}}{\Lambda}\left[\frac{r}{r_c}\right]^{\frac{1}{1+n}}\frac{1}{1 + \left[\frac{r}{L_c - 2r_c - r}\right]^{\frac{1}{1+n}} + \left[\left(\frac{r_d}{r_c}\right)\left(\frac{r}{\frac{1}{2}L_c - r_c - r_d - r}\right)\right]^{\frac{1}{1+n}}}. \tag{4}$$

When the number of secondary voids distributed homogeneously between the neighboring primary voids is N, Eq. (4) is changed to

$$\varepsilon_p = \frac{\varepsilon_{ij}^r}{\Lambda}\left[\frac{r}{r_c}\right]^{\frac{1}{1+n}}\frac{1}{1 + \left[\frac{r}{L_c - 2r_c - r}\right]^{\frac{1}{1+n}} + \sum_{s=0}^{N}\left[\left(\frac{r_d}{r_c}\right)\left(\frac{r}{\frac{1}{2}L_c - r_c - r_d - r - sL_d}\right)\right]^{\frac{1}{1+n}}}. \tag{5}$$

In uniaxil tensile condition, the incompatibility in shape change between aluminum matrix and dispersoids/precipitates incurs geometrically-necessary dislocations introduced to make up for the discrepancy (Ashby, 1970). The densities of geometrically-necessary dislocations around the sphere-shaped dispersoids and disc- or needle-shaped

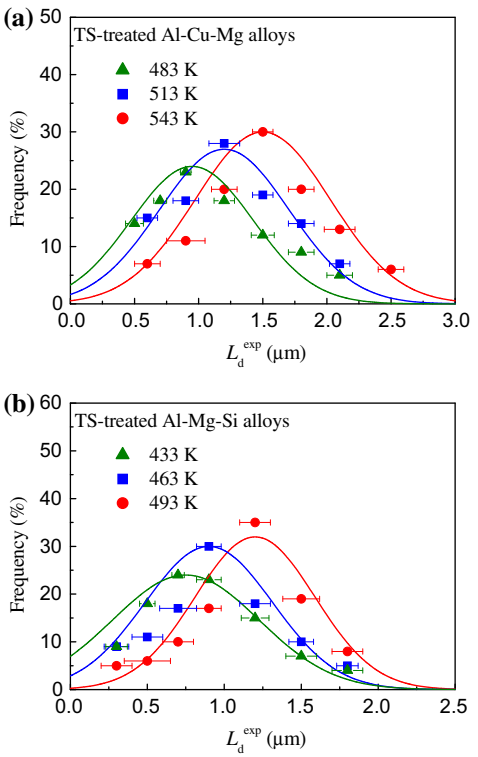

Fig. 5. Nearest neighbor spacing distribution of secondary voids (L_d^{exp}) in (a) TS-treated Al–Cu–Mg alloys peak-aged at different temperature and (b) TS-treated Al–Mg–Si alloys peak-aged at different temperature. Dots are experimental results and fitting curves are also presented.

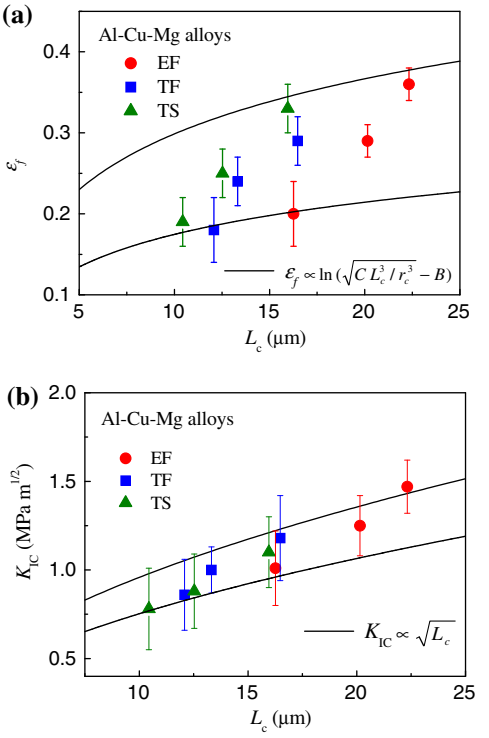

Fig. 6. Measurements on ductility with respect to the average intervoid spacing of primary voids for (a) Al–Cu–Mg alloys and (b) Al–Mg–Si alloys with different heat treatments. Curves are calculated by using Eqs. (16) and (17), respectively, and the upper and bottom ones are resulted from different scaling constants.

precipitates, ρ_d and ρ_p, are closely decided by the strains exerted on adjacent matrix bonded with the two populations of particles, ε^d and ε^p, respectively (Ashby, 1970; Brown and Stobbs, 1976):

$$\varepsilon^d = 1.7 r_d b \rho_d, \tag{6-1}$$

$$\varepsilon^p = 0.25 L_p b \rho_p \tag{6-2}$$

with b being Burgers vector of matrix and L_p the interparticle spacing of the precipitates. The ratio between ρ_d and ρ_p is associated with the ratio between interparticle spacings of the two populations of particles, L_d and L_p, as follows:

$$\frac{\rho_d}{\rho_p} = k \frac{L_p}{L_d}, \tag{7}$$

where k is a scaling factor and considered as unity here. Letting ρ_g be the sum of ρ_d and ρ_p, it plus the density of statistically-stored dislocations, ρ_s, comes to the total dislocation density in matrix, ρ_t

$$\rho_t = \rho_g + \rho_s, \tag{8}$$

A critical value of ρ_t, denoted as ρ_t^c, is assumed being existed and once ρ_t reaching this "dislocation limit" then material fractures regardless of how the detailed courses are (Liu et al, 2004). Neglecting constraint from second phase particles, ρ_t^c should be a constant by hypothesizing that the following engineering mechanical expression could applied effectively in micro scale of ligament:

$$\tau_m = \kappa G b \sqrt{\rho_t^c} \tag{9}$$

in which τ_m, the intrinsic shear strength of matrix, G, the shear modulus of matrix, together with b and κ all are constants for a given matrix such as aluminum. At the same time, ρ_s could be approximately considered as invariable because the increase in ρ_s is very inappreciable compared with that in ρ_g under external loading (Russell and Ashby, 1970). Therefore the criterion for fracture is further defined as ρ_g reaching the constant ρ_g^c:

$$\rho_g^c = \rho_t^c - \rho_s \tag{10}$$

From aforementioned analyses, Eq. (6) could be rewritten as:

$$\varepsilon_c^d = 1.7 r_d b \frac{L_p}{L_d + L_p} \rho_g^c, \tag{11-1}$$

$$\varepsilon_c^p = 0.25 L_p b \frac{L_d}{L_d + L_p} \rho_g^c. \tag{11-2}$$

The micro-plastic strain of $\tilde{\varepsilon}_{ij}$ in Eq. (4) is a combination of ε_c^d and ε_c^p in the form of Pythagorean theorem not of linear addition due to the existence of overlap effect between the two types of strains:

$$\tilde{\varepsilon}_{ij} = \sqrt{(\varepsilon_c^d)^2 + (\varepsilon_c^p)^2}. \tag{12}$$

Submitting Eq. (12) into Eq. (4) yields

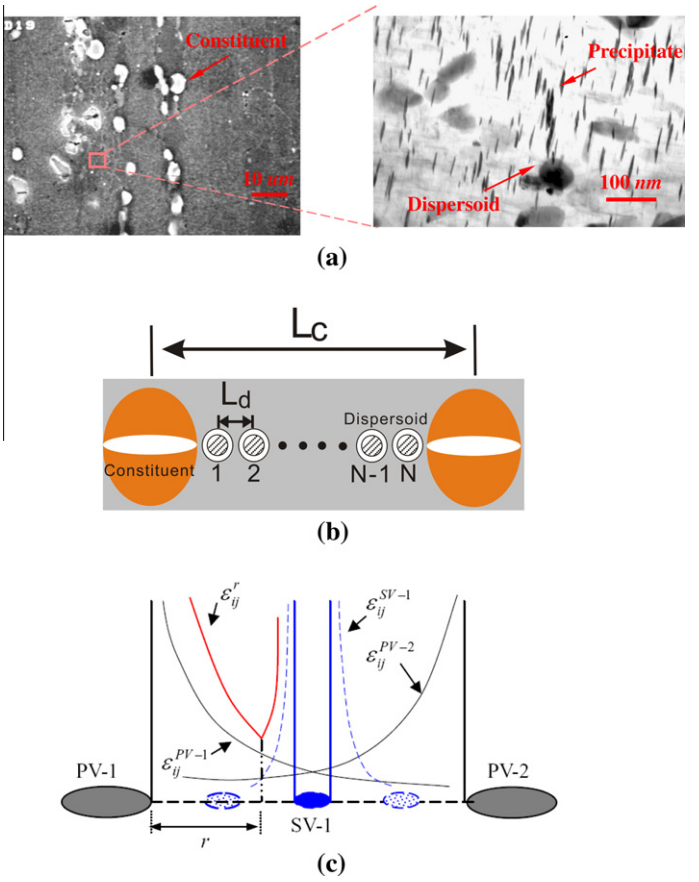

Fig. 7. (a) Typical SEM and TEM images showing the three types of second phase particles (constituents, dispersoids, and precipitates) with different size in Al–Mg–Si alloy. (b) Sketch illustrating the fracture mode in aluminum alloys that contain two populations of voids. The primary voids nucleate on the cracked constituents and the secondary voids nucleate on the decohered dispersoids. (c) Micromechanics model for ductile fracture of the aluminum alloys.

$$\varepsilon_p = \frac{b\rho_g^c}{\Lambda}\left[\frac{r}{r_c}\right]^{\frac{1}{1+n}} \frac{(L_d+L_p)^{-1}\sqrt{\left[(1.7r_dL_p)^2+(0.25L_dL_p)^2\right]}}{1+\left[\frac{r}{L_c-2r_c-r}\right]^{\frac{1}{1+n}}+\left[\left(\frac{r_d}{r_c}\right)\left(\frac{r}{\frac{1}{2}L_c-r_c-r_d-r}\right)\right]^{\frac{1}{1+n}}}. \tag{13}$$

At a location r where ε_p has a minimum value, the achievement of ρ_g^c indicates that the alloy will fracture fully (Liu et al., 2003a, 2004). The macro-plastic strain ε_f can be calculated from Eq. (13), equal to the minimum ε_p in variation with r. When the number of secondary voids homogeneously distributed between the neighboring primary voids is N, Eq. (13) is revised as

$$\varepsilon_f = \varepsilon_p|_{\min} = \frac{b\rho_g^c}{\Lambda}\left[\frac{r}{r_c}\right]^{\frac{1}{1+n}} \times \frac{(L_d+L_p)^{-1}\sqrt{\left[(1.7r_dL_p)^2+(0.25L_dL_p)^2\right]}}{1+\left[\frac{r}{L_c-2r_c-r}\right]^{\frac{1}{1+n}}+\sum_{s=1}^{N}\left[\left(\frac{r_d}{r_c}\right)\left(\frac{r}{\frac{1}{2}L_c-r_c-r_d-r-sL_d}\right)\right]^{\frac{1}{1+n}}} \tag{14}$$

The fracture toughness (K_{IC}) can be further obtained, according to its relationships with ε_f and σ_y (Garrett and Knott, 1978; Liu et al., 2003a)

$$K_{IC} = \sqrt{\frac{bn^2\rho_g^c E\sigma_y}{\Lambda(1-\nu)}\left[\frac{r}{r_c}\right]^{\frac{1}{1+n}} \frac{(L_d+L_p)^{-1}\sqrt{\left[(1.7r_dL_p)^2+(0.25L_dL_p)^2\right]}}{1+\left[\frac{r}{L_c-2r_c-r}\right]^{\frac{1}{1+n}}+\sum_{s=1}^{N}\left[\left(\frac{r_d}{r_c}\right)\left(\frac{r}{\frac{1}{2}L_c-r_c-r_d-r-sL_d}\right)\right]^{\frac{1}{1+n}}}}, \tag{15}$$

where E and ν are the elastic modulus and Poisson's ratio of the Al matrix. The above two equations, i.e., Eqs. (14) and (15), quantitatively show the dependence of ductility and fracture toughness of the aluminum alloys on the combination of primary voids and secondary voids. Because the absolute values of some parameters, such as ρ_g^c and $\tilde{\varepsilon}_e(\theta)$, are difficulty to determine while all of these parameters could be regarded as constants approximately, the strain to fracture and fracture toughness calculated here are normalized, *i.e.*, divided by a reference strain to fracture (ε_f^R) and fracture toughness (K_{IC}^R), respectively, to eliminate these unknown parameters, as treated in our previous works (Liu et al, 2003a, 2004, 2005, 2007).

It is well known (Lloyd, 2003) that, because the strain rate sensitivity in Al alloys is too low to provide any resistance to strain localization, the Al alloys fracture quickly once the mechanical instability attained. The present model is thus reasonable even considering no strain localization. Using Eqs. (14) and (15), the combined influence of

primary and secondary voids on both ε_f and K_{IC} can be calculated. As mentioned before, reference ε_f^R and K_{IC}^R should be firstly chosen and normalization treatments were subsequently performed to yield the normalized ε_f and K_{IC} (Liu et al., 2003a, 2004, 2005, 2007). The ε_f^R and K_{IC}^R used in present paper are the ε_f and K_{IC} of the TF-treated Al–Cu–Mg alloys peak-aged at 513 K and the TF-treated Al–Mg–Si alloys peak-aged at 463 K, respectively.

Fig. 8(a) and (b) shows some calculated ductility contours (lines) of the Al–Cu–Mg and Al–Mg–Si alloys in variants of the primary voids (L_c) and secondary voids (L_d), respectively. All the combined effects of L_c and L_d on a contour should put out the same ductility. These contours were obtained by calculating different combinations of primary voids and secondary voids, i.e., $L_c \in (5.0, 30.0)$ μm and $L_d \in (0, 1.5)$ μm and all points with the same ductility form a contour. It is clearly shown that the ductility is sensitive not only to the primary voids but also to the secondary voids. The presence of secondary voids will reduce the ductility and even cause the alloys containing less primary voids exhibit inferior ductility. Taking the comparison between point A and B (Fig. 8(a)) for example, point A has ductility (normalized $\varepsilon_f = 1.25$) larger than point B (normalized $\varepsilon_f = 1.0$), although the former has more primary voids (or cracked constituents) (L_c of point A and B is about 17.5 and 20.0 μm, respectively). This is because the secondary voids in point B are much more than in point A (L_d of point A and B is about 0.95 and 0.50 μm, respectively) and the remarkable influence of secondary voids makes point B exhibit ductility inferior to point A. These results indicate that only reducing the constituent content is not enough to enhance the fracture properties of commercial heat-treatable aluminum alloys, suitable controlling of the homogenization and solution treatments is also required to ensure the good fracture properties because the dispersoids will evolve during these two heat treatments, causing difference in secondary voids. On the other hands, Fig. 8 also shows that, if the practically produced constituent density (primary void density) exceeds the designed one (which means a resultant reduction in L_c and in ductility), the fracture properties may be repaired by decreasing the dispersoid density (decreasing secondary void density or increasing L_d), which can be carefully tailored in homogenization or solution treatments.

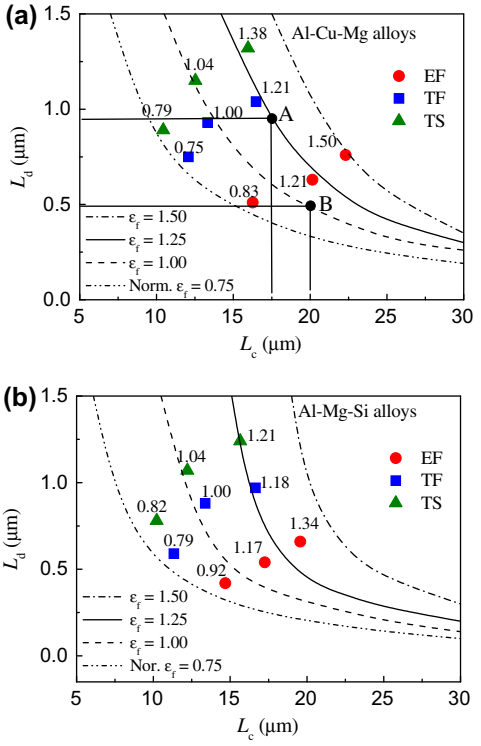

Fig. 8. Some contours of the ductility of the (a) Al–Cu–Mg alloy and (b) Al–Mg–Si alloys in variants of the average intervoid spacing of both primary voids and secondary voids. All the dots are experimental results and the curves are calculated results. The reference ductility, ε_f^R, is that of the TF-treated sample peak-aged at 513 K and 463 K for the Al–Cu–Mg alloy and the Al–Mg–Si alloy, respectively.

Many researchers have studied the influence of coarse particles on the ductility of metal materials and some models have been also developed to relate the (cracked) particle percentage to the ductility quantitatively (see, e.g., Goods and Brown, 1979; Thompson, 1975). Brown and Embury (1973) have suggested that the relationship between the ductility and the particles acting as void nuclei could be expressed as

$$\varepsilon_f \propto \ln\left(\sqrt{A/f_c} - B\right) \propto \ln\left(\sqrt{CL_c^3/r_c^3} - B\right), \tag{16}$$

where A, B, and C all are constants and f_c is the volume fraction of cracked coarse particles. It is shown from above expression that more (cracked) particles and/or larger particles should result in lower ductility. This is applicable to many metals and alloys where the ductile fracture is predominantly controlled by the coarse particles. However, when applied to the aluminum alloys where the influence of secondary voids should not be neglected, Eq. (16) is no longer satisfactory because of the lack of secondary voids. The calculations from Eq. (16) are shown in Fig. 6(a) as lines. One can see that the calculations are not in good agreement with the experiments. Especially, the unusual experimental phenomenon that some alloys containing more primary voids have higher ductility can not be reasonably explained. On the other hand, the experiment results can be well modeled by present model when both the primary voids and secondary voids are considered simultaneously, see Fig. 8. This indicates that the consideration on both primary voids and secondary voids should be necessary in order to well understand the ductile fracture of aluminum alloys.

Fracture toughness is another important mechanical property that is sensitive to the second phase particles. A well known expression has been proposed by Hahn and Rosenfield (1975) to relate the fracture toughness to the cracked coarse particles, which is given as

$$K_{IC} \propto (f_c)^{-1/6} \propto \sqrt{L_c}. \tag{17}$$

This expression is found to fit well with the present experimental results (Fig. 6(b)). It seems that the fracture toughness is predominantly controlled by the coarse particles or

the primary voids. However, it will be revealed that this conclusion must be treated with caution when referring to the combined effect of primary voids and secondary voids on the fracture toughness as shown in Fig. 9. The lines in Fig. 9 are some calculated fracture toughness contours in variants of the primary voids (L_c) and secondary voids (L_d). When L_d is larger than about 0.5 μm, the fracture toughness is most sensitive to L_c. When the secondary voids increase and L_d reduces down to less than 0.5 μm, the influence of secondary voids is significant. In other words, how the secondary voids can affect the fracture toughness is dependent on the mount of the secondary voids.

As mentioned above, the secondary voids in aluminum alloys are caused by the dispersoid decohesion. The dispersoid decohesion is related to many factors, such as the dispersoid size, dispersoid/matrix interfacial strength, etc. Experiments (Chen and Knott, 1981) have shown that the aluminum alloys containing $ZrAl_3$ dispersoids had fracture toughness superior to the aluminum alloys containing $Al_{18}Cr_2Mg_3$ dispersoids, because the semicoherent $ZrAl_3$ dispersoids have a larger interfacial strength than the $Al_{18}Cr_2Mg_3$ dispersoids. This can be well explained in present model. It have been generally known that a higher dispersoid/matrix interfacial strength will prevent more dispersoids from decohesion, resulting in larger L_d and concomitant higher fracture toughness (Fig. 9).

The coupling effect of the two voids on the ductility and fracture toughness is significantly sensitive to the matrix strength, as clearly demonstrated in Figs. 8 and 9. With the increase in strength, such as the case on EF-treated Al–Cu–Mg alloys indicated by arrow in Fig. 9 (the values in brackets are the yield strength), the two voids evolve and the combined effect of the two voids shifts both the ductility and fracture toughness to lower value contours. The development of the contours means that it is possible to tailor the two voids by artificially controlling the aging treatments to achieve superior ductility and fracture toughness.

It has proposed (Lloyd, 2003) that there exist a scaling relationship between the tensile ductile fracture strain (taken as the reduction in area at fracture, φ) and the yield strength in aluminum alloys. Here in present experiments, we find that this relationship is applicable to all the alloys with different heat treatments, as shown in Fig. 10. This further indicates that the ductile fracture of aluminum alloys should be intrinsically related to the strength, essentially similar to what revealed from present model. One can also find from Fig. 10 that, with reducing the constituents/dispersoids and simultaneously increasing the strengthening precipitates, the scaling lines of the two aluminum alloys both shift to the right. The shift of scaling lines with solution + quench treatments is caused by the change in "microstructure" (in this case refer to those microstructural features that would produce a change in the fracture behaviors) because the relative volume fraction among the three kinds of second phase particles have been changed after the different solution + quench treatments.

Finally, it should be mentioned that the model and approaches presented in this work are applicable not only to the current Al–Cu–Mg and Al–Mg–Si alloys, but also to almost all the aluminum alloys or aluminum-based composites that fracture through coalescence of voids. A shortcoming of present model is the simple assumption of the cubic arrangement of the primary voids, while in practical aluminum alloys the constituents and the resultant primary voids are randomly distributed. This simple assumption will surely cause some differences between the predictions and the experimental results. However, these

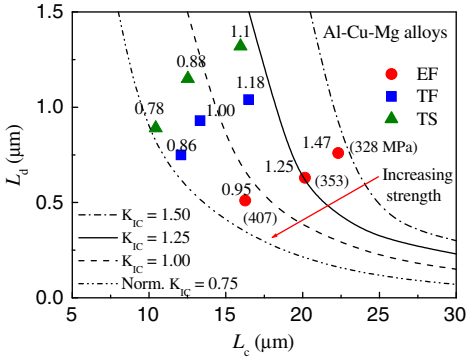

Fig. 9. Some contours of the fracture toughness of the Al–Cu–Mg alloy in variants of the average intervoid spacing of both primary voids and secondary voids. All the dots are experimental results and the curves are calculated results. The reference ductility, K_{IC}^R, is that of the TF-treated sample peak-aged at 513 K.

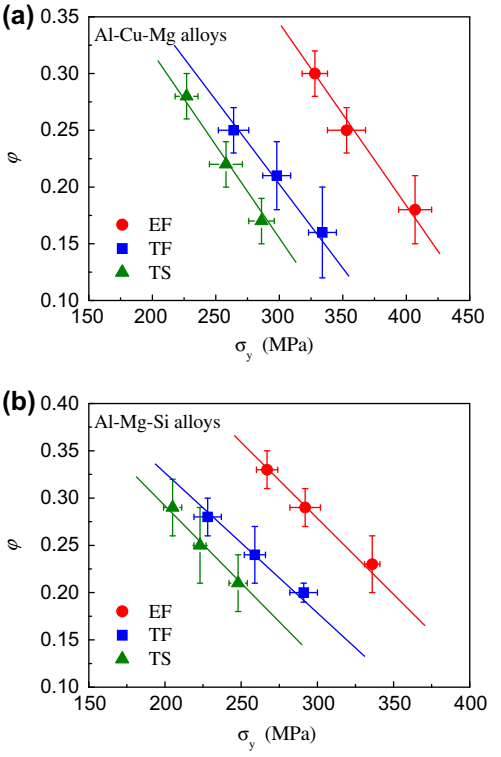

Fig. 10. Scaling relationship between the reduction in area at fracture, φ, and the yield strength in (a) Al–Cu–Mg alloys and (b) Al–Mg–Si alloys.

differences can be reduced by using the normalization treatment (Liu, 2002), where all constant parameters are removed. Further work is needed to improve the model by more precisely describing the distribution of the primary voids.

5. Conclusions

(1) It is clearly revealed from experiments and modeling that the ductility and fracture toughness of aluminum alloys are dependent not only on the primary voids but also on the secondary voids and the combined effect of the two voids is related to the matrix strength. The presence of secondary voids reduces the ductility and fracture toughness and even makes the alloys containing less primary voids exhibit inferior ductile properties.

(2) A model based on fracture mechanics has been developed to quantitatively calculate the coupling effect of two voids on the ductility and fracture toughness of aluminum alloys. Calculations are in good with experimental results on Al–Cu–Mg alloys and Al–Mg–Si alloys. Further predictions from present modeling show that, when the intervoid spacing of the secondary voids is less than about 0.5 μm, the influence of secondary voids will be more intense;

(3) Contours of ductility and fracture toughness in variant with primary voids and secondary voids have been respectively developed for heat-treatable aluminum alloys, where the influence of matrix strength is illustratively shown. These can be used to aid the artificial controlling of aging treatment to tailor the combined effect of two voids, in order to achieve superior ductility and fracture toughness.

Acknowledgements

Supports by German Science Foundation under Grant Ec 111/16-2, the National Basic Research Program of China (Grant No. 2010CB631003), and the National Natural Science Foundation (50701035) are gratefully acknowledged. G. Liu and R. Li are grateful to the Alexander von Humboldt foundation for financial support.

References

Ashby, M.F., 1970. The deformation of plastically non-homogenous materials. Philosophical Magazine 21, 399–424.

Bandstra, J.P., Koss, D.A., 2001. Modeling the ductile fracture process of void coalescence by void-sheet formation. Materials Science and Engineering, 490–495.

Brocks, W., Sun, D.Z., Hönig, A., 1995. Verification of the transferability of micromechanical parameters by cell model calculations with visco-plastic materials. International Journal of Plasticity 11, 971–989.

Broek, D., 1973. Role of inclusions in ductile fracture and fracture toughness. Engineering Fracture Mechanics 5, 55–66.

Brown, L.M., Embury, J.D., 1973. The microstructure and design of alloys. In: Proceeding of the Third International Conference on the Strength of Metals and Alloys. The Institute of Metals, Cambridge, pp. 64–182.

Brown, L.M., Stobbs, W.M., 1976. Work-hardening of copper-sinica-5, equilibrium plastic relaxation by secondary dislocations. Philosophical Magazine 34, 351–364.

Chen, C.Q., Knott, J.F., 1981. Effects of dispersoid particles on toughness of high-strength aluminum alloys. Metal Science 15, 357–364.

Fabregue, D., Pardoen, T., 2008. A constitutive model for elastoplastic solids containing primary and secondary voids. Journal of the Mechanics and Physics of Solids 56, 719–741.

Faleskog, J., Shih, F.C., 1997. Micromechanics of coalescence—I: Synergistic effects of elasticity, plastic yielding and multi-size-scale voids. Journal of the Mechanics and Physics of Solids 45, 21–25.

Garrett, G.G., Knott, J.F., 1978. Influence of compositional and microstructural variation on mechanism of static fracture in aluminum alloys. Metallurgical and Materials Transaction A 9A, 1187–1201.

Goods, S.H., Brown, L.M., 1979. The nucleation of cavities by plastic deformation. Acta Metallurgica 27, 1–15.

Hahn, G.T., Rosenfield, A.R., 1975. Metallurgical factors affecting fracture toughness of aluminum alloys. Metallurgical and Materials Transaction A 6A, 653–668.

Haynes, M.J., Gangloff, R.P., 1998. Temperature-dependent void-sheet fracture in Al–Cu–Mg–Ag–Zr. Metallurgical and Materials Transaction A 29A, 1599–1613.

Hornbogen, E., Starke, Jr. E.A., 1993. Theory assisted design of high strength low alloy aluminum. Acta Metallurgica et Materialia 41, 1–16.

Hutchinson, J.W., 1968. Singular behavior at the end of a tensile crack in a hardening material. Journal of the Mechanics and Physics of Solids 16, 13–31.

Liu, G., 2002. Modeling the quasi-static mechanical properties of aged aluminum alloys containing multi-scaled second phases. Ph. D Thesis. Xi'an Jiaotong University.

Liu, G., Zhang, G.J., Ding, X.D., Sun, J., Chen, K.H., 2003a. Dependence of fracture toughness on multiscale second phase particles in high strength aluminum alloys. Materials Science and Technology 19, 887–896.

Liu, G., Zhang, G.J., Ding, X.D., Sun, J., Chen, K.H., 2003b. Modeling the strengthening response to aging processing of heat-treatable aluminum alloys containing plate/disc or rod/needle-shaped precipitates. Materials Science and Engineering A344, 113–124.

Liu, G., Zhang, G.J., Ding, X.D., Sun, J., Chen, K.H., 2004. Influence of multiscale-sized second phase particles on ductility of aged aluminum alloys. Metallurgical and Materials Transaction 35A, 1725–1734.

Liu, G., Sun, J., Nan, C.W., Chen, K.H., 2005. Experiment and multiscale modeling of the coupled influence of constituents and precipitates on the ductile fracture of heat-treatable aluminum alloys. Acta Materialia 53, 3459–3468.

Liu, G., Zhang, G.J., Wang, R.H., Hu, W., Sun, J., Chen, K.H., 2007. Heat treatment-modulated coupling effect of multi-scale second-phase particles on the ductile fracture of aged aluminum alloys. Acta Materialia 55, 273–284.

Lloyd, D.J., 2003. The scaling of the tensile ductile fracture strain with yield strength in Al alloys. Scripta Materialia 48, 341–344.

Rice, J.R., Rosengren, G.F., 1968. Plane strain deformation near a crack tip in a power-law hardening material. Journal of the Mechanics and Physics of Solids 16, 1–12.

Russell, L.M., Ashby, M.F., 1970. Slip in aluminum crystal containing strong, plate like particles. Acta Metallurgica 18, 891–901.

Staley, J.T., 1979. Influence of microstructure on fatigue and fracture of aluminium alloys. Aluminum 55, 277–281.

Thompson, D.S., 1975. Metallurgical factors affecting high strength aluminum alloy production. Metallurgical and Materials Transaction A 6A, 671–683.

Tvergaard, V., 1998. Interaction of very small voids with larger voids. International Journal of Solids and Structures 35, 3989–4000.

Van Stone, R.H., Psioda, J.A., 1975. Discussion of "metallurgical factors affecting fracture toughness of aluminum alloys". Metallurgical and Materials Transaction A 6A, 668–670.

Walsh, J.A., Jata, K.V., Starke Jr., E.A., 1989. The influence of Mn dispersoid content and stress state on ductile fracture of 2134 type Al alloys. Acta Metallurgica 37, 2861–2871.

Yuan, S.P., Liu, G., Wang, R.H., Pu, X., Zhang, G.J., Sun, J., Chen, K.H., 2007. Coupling effect of multiple precipitates on the ductile fracture of Al–Mg–Si alloys. Scripta Materialia 57, 865–868.